Cellular/Molecular

Synaptic Input and ACh Modulation Regulate Dendritic Ca^{2+} Spike Duration in Pyramidal Neurons, Directly Affecting Their Somatic Output

Amir Dudai, Michael Doron, Idan Segev, and Michael London
The Edmond and Lily Safra Center for Brain Sciences (ELSC) and The Department of Neurobiology, The Life Sciences Institute, The Hebrew University of Jerusalem, Jerusalem, Israel 91904

Nonlinear synaptic integration in dendrites is a fundamental aspect of neural computation. One such key mechanism is the Ca^{2+} spike at the apical tuft of pyramidal neurons. Characterized by a plateau potential sustained for tens of milliseconds, the Ca^{2+} spike amplifies excitatory input, facilitates somatic action potentials (APs), and promotes synaptic plasticity. Despite its essential role, the mechanisms regulating it are largely unknown. Using a compartmental model of a layer 5 pyramidal cell (L5PC), we explored the plateau and termination phases of the Ca^{2+} spike under input current perturbations, long-step current-injections, and variations in the dendritic high-voltage-activated Ca^{2+} conductance (that occur during cholinergic modulation). We found that, surprisingly, timed excitatory input can shorten the Ca^{2+} spike duration while inhibitory input can either elongate or terminate it. A significant elongation also occurs when the high-voltage-activated Ca^{2+} channels (Ca_{HVA}) conductance is increased. To mechanistically understand these phenomena, we analyzed the currents involved in the spike. The plateau and termination phases are almost exclusively controlled by the Ca_{HVA} inward current and the I_m outward K^+ current. We reduced the full model to a single-compartment model that faithfully preserved the responses of the Ca^{2+} spike to interventions and consisted of two dynamic variables: the membrane potential and the K^+-channel activation level. A phase-plane analysis of the reduced model provides testable predictions for modulating the Ca^{2+} spike and reveals various dynamical regimes that explain the robust nature of the spike. Regulating the duration of the Ca^{2+} spike significantly impacts the cell synaptic-plasticity window and, as we show, its input-output relationship.

Key words: **Ca^{2+} spike; dendrites; phase plane; synaptic perturbation**

Significance Statement

Pyramidal neurons are the cortex's principal projection neurons. In their apical tuft, dendritic Ca^{2+} spikes significantly impact information processing, synaptic plasticity, and the cell's input-output relationship. Therefore, it is essential to understand the mechanisms regulating them. Using a compartmental model of a layer 5 pyramidal cell (L5PC), we explored the Ca^{2+} spike responses to synaptic perturbations and cholinergic modulation. We showed a counterintuitive phenomenon: early excitatory input shortens the spike, whereas weak inhibition elongates it. Also, we demonstrated that acetylcholine (ACh) extends the spike. Through a reduced model containing only the membrane potential and the K^+-channel activation level, we explained these phenomena using a phase-plane analysis. Our work provides new information about the robustness of the Ca^{2+} spike and its controlling mechanisms.

Introduction

The dendrites of neocortical and hippocampal pyramidal neurons contain a host of voltage-dependent ion channels supporting a rich repertoire of electrical behavior in response to synaptic inputs. For example, the apical dendrites express voltage-dependent Na^+ channels that support back-propagation of action potentials (APs; Stuart and Sakmann, 1994). Another mechanism involves the local dendritic generation of NMDA spikes which play a key role in computational mechanisms and plasticity (Larkum et al., 2009; Major et al., 2013; Doron et al., 2017). Undoubtedly, however, the most dramatic of these dendritic

Received July 18, 2021; revised Nov. 25, 2021; accepted Nov. 29, 2021.

Author contributions: A.D., M.D., and M.L. designed research; A.D. and M.D. performed research; A.D. contributed unpublished reagents/analytic tools; A.D. analyzed data; A.D. wrote the first draft of the paper; A.D., I.S., and M.L. edited the paper; A.D. and M.L. wrote the paper.

This work was supported by the Israeli Science Foundation Grant 1024/17, the Einstein Foundation (M.L.), and the Gatsby Charitable Foundation. A.D. is an H. & S. Hoffman fellow. M.L. is a Sachs Family Lecturer in Brain Science.

The authors declare no competing financial interests.

Correspondence should be addressed to Michael London at mickey.london@mail.huji.ac.il.

https://doi.org/10.1523/JNEUROSCI.1470-21.2021

events is the Ca^{2+} spike, which takes place in the cell's nexus (Reuveni et al., 1993; Schiller et al., 1997; Stuart and Spruston, 2015). These Ca^{2+} spikes generate a huge depolarization in the dendrites, which lasts for tens of milliseconds and is accompanied by a significant influx of Ca^{2+} ions into the cell. The dendritic depolarization associated with the Ca^{2+} spike often affects the somatic region and leads to a short burst of axonal APs (Leleo and Segev, 2021). Functionally, Ca^{2+} spikes were shown to play a central role in the transmission of higher-level top-down signals, the coupling between the soma and the apical tuft, and the modulation of synaptic plasticity (Larkum et al., 1999, 2001; Stuart and Häusser, 2001; Golding et al., 2002; Spruston, 2008; Bittner et al., 2017; Poleg-Polsky, 2019; Suzuki and Larkum, 2020; Takahashi et al., 2020). Modern compartmental models were able to replicate the nonlinear Ca^{2+} spike phenomenon (Hay et al., 2011; Shai et al., 2015); however, a fundamental understanding of its underlying mechanism and how various factors can modulate it is still lacking because of challenges involved in characterizing multiple ion channel dynamics simultaneously, while accounting for unknown channel densities.

Despite these challenges, numerous physiological and modeling studies have demonstrated that various biological factors can control the voltage waveform of the Ca^{2+} spike. Such factors include the specific geometry of the dendritic tree and the specific composition of ion channels it contains (Golding et al., 1999; Vetter et al., 2001; Schaefer et al., 2003; Hay et al., 2011; Harnett et al., 2013, 2015; Fletcher and Williams, 2019; Galloni et al., 2020). Inhibitory synapses and neuromodulatory signals also shape the active dendritic properties of pyramidal cells, influencing the excitability of the apical dendrites and the coupling between the soma and the nexus (Larkum et al., 1999; Gidon and Segev, 2012; Palmer et al., 2012; Pérez-Garci et al., 2013; Labarrera et al., 2018; Williams and Fletcher, 2019). Because of the relatively long duration of the dendritic Ca^{2+} spike, various manipulations and synaptic input perturbations may alter its stereotypical voltage waveform. Thus, each of these manipulations can directly affect local plasticity, the communication between the soma and the nexus, and the overall output of the cell. Therefore, examining the response properties of the Ca^{2+} spike to various biophysical modulations can provide key insights into information processing in the neocortex.

A typical Ca^{2+} spike voltage waveform can be roughly divided into three phases: initiation, plateau potential, and termination (Fig. 1). The initiation phase of the Ca^{2+} spike involves the interaction of many ion channels, and it highly depends on the specific stimulation that initiated the spike. Therefore, here we focus on the plateau potential and the termination phases of the spike and explain the underlying mechanisms that control them. Then, we examine how different biophysical manipulations and perturbations affect the Ca^{2+} spike in a model of layer 5 pyramidal cell (L5PC). We next generate a reduced single-compartment model with two biologically-relevant variables in which the induced modulations are conserved; this enables us to explain the Ca^{2+} spike dynamics and its robust responses to perturbations through a 2D dynamical system with which we can predict the effect of further interventions. Finally, we construct a two-compartment model consisting of a nexus and a soma to observe the direct influence these manipulations have on the number of APs, the output of the cell.

Materials and Methods

NEURON models and simulations

We used the NEURON 7.7 simulation module in Python to perform the L5PC simulations in this work (Carnevale and Hines, 2006), along with

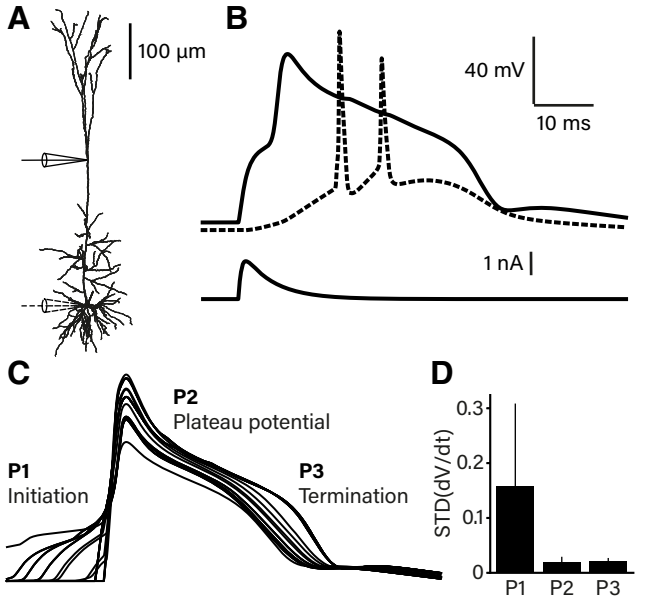

Figure 1. Ca^{2+} spike typicality. ***A***, Morphology of L5PC model along with the current injection and recording sites (solid line: nexus; dashed line: soma). ***B***, Voltage traces of the nexus and the soma during a Ca^{2+} spike (top) following a brief synaptic-like depolarizing current injection (bottom). ***C***, Ca^{2+} spike voltage traces generated following various stimuli combinations. The Ca^{2+} spike can be divided into three phases: (P1) initiation, (P2) plateau potential, and (P3) termination. ***D***, Quantification of the variability in trace shape for each phase in the voltage waveform, in response to a range of current stimuli.

self-written scripts in Python for the reduced model and dynamical analysis. The code for generating all the figures and simulations is available at https://github.com/amirdud/Ca_spike_modulation. The full L5PC compartmental model used in this study was developed by Hay et al. (2011) and later updated by Shai et al. (2015; channels and morphology; available at ModelDB: https://senselab.med.yale.edu/ModelDB/showmodel.cshtml?model=139653#tabs-1 and https://senselab.med.yale.edu/ModelDB/ShowModel?model=180373#tabs-1, respectively). We also modified the I_h channel dendritic distribution, as in Labarrera et al. (2018). The L5PC model is composed of soma, axonal, basal and apical sections (~200 compartments). Across the cell model there are ten voltage-dependent channels (seven in the apical dendritic tree) and internal variables controlling the Ca^{2+} dynamics (see Hay et al., 2011, for the specific parameters used for each variable). To examine the Ca^{2+} spike typicality in the L5PC model (Fig. 1), we stimulated the soma and the nexus with various current combinations: the soma was stimulated with current steps ranging between 0 and 4 nA (lasting either 4 or 5 ms), and the nexus was stimulated with EPSC-like double-exponent current: 0.5-ms rise time, 5-ms decay time, ranging between 0- and 3-nA peak current (with 0- to 5-ms delay from the end of the soma stimulation). The standard deviation of the voltage waveform derivatives was calculated at each time point in the three phases (10 ms for each phase).

Current perturbations and modulations of the L5PC model

The Ca^{2+} spike in the full L5PC model (in Fig. 2) was initiated with an EPSC-like current in the nexus with the following parameters: 0.5-ms rise time, 5-ms decay time, and 1.6-nA peak current. The perturbation currents had similar time constants with peak current intensity ranging from −1 to 1 nA (with onset delay of 5–25 ms relative to initiation). The perturbation currents were dispersed across all apical dendrites, where the peak intensity of each synapse was relative to each segment surface area. The spike time duration was calculated at voltages above −40 mV. For eliminating the APs, we set the somatic and axonal Na^+ and Ca^{2+} conductances to 0. The DC constant current stimulation ranged between 0.8 and 2.6 nA, and each was spread across all neuronal segments

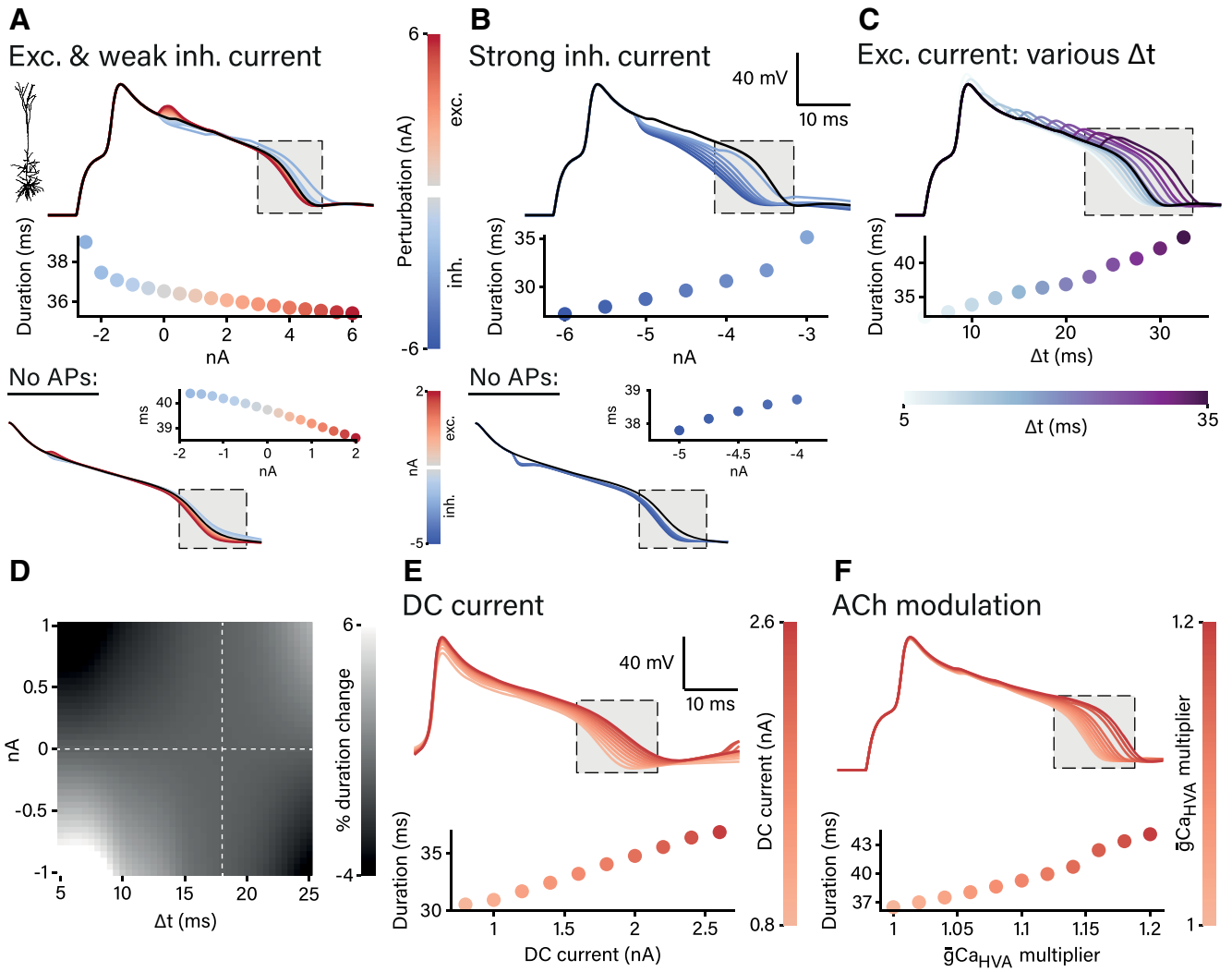

Figure 2. Perturbing and modulating the L5PC Ca^{2+} spike. ***A***, Changes in Ca^{2+} spike duration following a double-exponential-current perturbation (15 ms postinitiation) with either excitatory currents (reds) or weak inhibitory currents (blues). Top, Ca^{2+} spike voltage traces (black trace: nonperturbation; shaded area: termination), and a quantification of the Ca^{2+} spike duration as a function of the perturbation-current peak. Bottom, Perturbations with no somatic APs. ***B***, Same as ***A*** with a strong inhibitory current. ***C***, Same as ***A*** top, with excitatory currents at different perturbation timings. ***D***, Change in Ca^{2+} spike duration (%) as function of the perturbation-current peak and the perturbation timing (dashed lines: sign transition in duration). ***E***, Same as ***A*** top, with constant DC current at various stimulation amplitudes. ***F***, Same as ***A*** top, with an increase in the Ca_{HVA} conductance at the apical dendrites.

(relative to the segment surface area). In the high-voltage-activated Ca^{2+} channels (Ca_{HVA}) peak conductance experiments, the values of $\bar{g}_{Ca_{HVA}}$ in the apical dendritic segments were multiplied by a factor ranging between 1 and 1.2.

Reduced models

The morphologically reduced model (Fig. 3) consisted of all nexus channels in the full L5PC model with similar peak conductance values and Ca^{2+} dynamic parameters (with 10-μm soma diameter). To initiate a Ca^{2+} spike in this model, we used the following parameters: 0.5-ms rise time, 5-ms decay time, and 0.03-nA peak current. The physiologically reduced model (Fig. 4) was self-written in Python, where the system of differential equations was solved using the odeint function in the Scipy module (1.5.2). We first reduced the model to four variables, including the membrane voltage and the dynamic variables of the I_m and Ca_{HVA} currents ($V, n_{I_m}, m_{Ca_{HVA}}$ and $h_{Ca_{HVA}}$). The maximal conductances of I_m and Ca_{HVA} were increased and balanced to compensate for the loss of the other currents in the model (5:7.5, respectively) to $\bar{g}_{I_m}$ = 7.4 mS/cm^2 and $\bar{g}_{Ca_{HVA}}$ = 3.5 mS/cm^2. The following parameters were used to model the Ca_{HVA} gating variables (same as Reuveni et al., 1993; Hay et al., 2011):

$$\alpha_m = \frac{0.055 \cdot (-27-V)}{\exp((-27-V)/3.8)-1}; \quad \beta_m = 0.94 \cdot \exp((-75-v)/17)$$

$$\alpha_h = 0.000457 \cdot \exp((-13-V)/50);$$

$$\beta_h = \frac{0.0065}{\exp((-V-15)/28)+1}.$$

The parameters used to model the I_m gating variable (same as Adams et al., 1982; Hay et al., 2011):

$$\alpha_n = 0.0033 \cdot \exp(0.1 \cdot (V-35));$$
$$\beta_h = 0.0033 \cdot \exp(-0.1 \cdot (V-35)).$$

We calculated τ_i and i_∞ for each gating variable (where $i \in \{m_{Ca_{HVA}}, h_{Ca_{HVA}}, n_{I_m}\}$) using the following formulas:

$$\tau_i(V) = \frac{1}{\alpha_i(V)+\beta_i(V)}; \quad i_\infty = \frac{\alpha_i(V)}{\alpha_i(V)+\beta_i(V)}.$$

The reversal potentials of the ion channels were E_K = −77 mV and E_{Ca} = 132 mV, the specific capacitance was 1 μF/cm^2 and the diameter of the cell 18 μm. To initiate a Ca^{2+} spike in this model, we used the

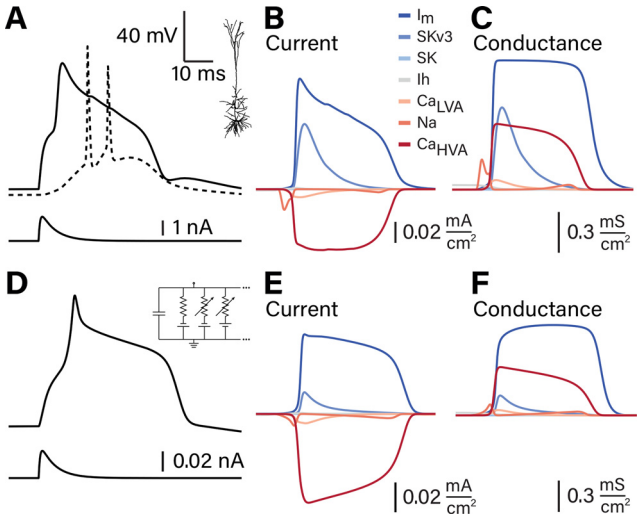

Figure 3. Similar membrane currents underlie the L5PC Ca^{2+} spike and the corresponding single-compartment nexus model. ***A***, Voltage traces of the soma (dashed line) and the nexus (solid line) following Ca^{2+} spike initiation in the L5PC model. ***B***, The membrane currents involved in the Ca^{2+} spike in ***A***, sorted by their peak current amplitude. ***C***, The conductances involved in the Ca^{2+} spike in ***A***. ***D–F*** are the same as ***A–C***, respectively, for the single-compartment iso-potential nexus model.

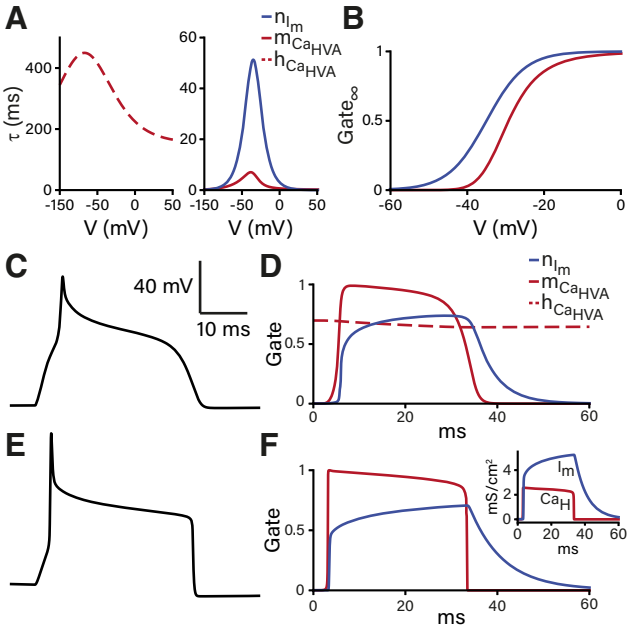

Figure 4. Reducing the Ca^{2+} spike model to two biological variables (V and n_{I_m}). ***A***, The time constants of the Ca_{HVA} and I_m gating variables. Left, $h_{Ca_{HVA}}$. Right, $m_{Ca_{HVA}}$ (red) and n_{I_m} (blue). ***B***, Activation curves of $m_{Ca_{HVA}}$ and n_{I_m} (at $t = \infty$). ***C***, Ca^{2+} spike dynamics of a model that includes all the three gates shown in ***A***. ***D***, The dynamics of $h_{Ca_{HVA}}$ (dashed red), $m_{Ca_{HVA}}$ (solid red), and n_{I_m} (blue) for the model in ***C***. ***E***, Same as ***C*** but for a model with two dynamic variables: V and n_{I_m}. ***F***, The dynamics of $m_{Ca_{HVA}}$ and n_{I_m} for the model in ***E***. Inset, The conductances of the two channels in the model.

following parameters: 0.5-ms rise time, 5-ms decay time, and 0.4-nA peak current. In the two-variable reduced model, we used V and n_{I_m} as the dynamic variables with first-order dynamics of $m_{Ca_{HVA}\infty}$ and constant value for $h_{Ca_{HVA}\infty}$. The parameters of I_m were slightly modified for better replicating the Ca^{2+} spike dynamics:

$$\alpha_n = 0.002 \cdot \exp(0.092 \cdot (V + 39));$$

$$\beta_n = 0.002 \cdot \exp(-0.092 \cdot (V + 39)).$$

The reversal potentials of the currents were $E_K = -85$ mV and $E_{Ca} = 120$ mV. To initiate a Ca^{2+} spike in this model, we used the following parameters: 0.5-ms rise time, 5-ms decay time, and 0.4-nA peak current.

In Figure 5, this two-variable reduced model was perturbed 15 ms following the Ca^{2+} spike initiation with currents that ranged between −0.9 and 0.5 nA (with onset delay of 10–30 ms relative to initiation). The DC current intensity ranged between 0.02 and 0.12 nA. The maximal conductance of Ca_{HVA} was multiplied by a factor between 1 and 1.1 in the cholinergic modulation experiments.

2D dynamical system

The V and n_{I_m} nullclines (Fig. 6) were found by setting the time derivatives of the dynamic variables (dV/dt and dn_{I_m}/dt, respectively) to 0 to get the following expressions:

$$V\text{-nullcline: } n_{I_m} = (I_{ext} - \bar{g}_{Ca_{HVA}} m_{Ca_{HVA_\infty}}(V) h_{Ca_{HVA_\infty}}(V_0)(V - E_{Ca}) - g_L(V - E_L))/\bar{g}_{I_m}(V - E_K)$$

$$n_{I_m}\text{-nullcline: } n_{I_m} = \alpha_n(V)/(\alpha_n(V) + \beta_n(V)).$$

The time derivative arrows were calculated for V values between −120 and 50 mV and n_{I_m} values between 0 and 1. The initial values for initiating the Ca^{2+} spike were $V = -30$ mV and $n_{I_m} = 0$. In Figure 7, the nonperturbed trajectories were initiated with $V = -30$ mV and $n_{I_m} = 0$, 0.1, and 0.2. The {voltage shift (mV), perturbation timing (ms)} pairs of the regeneration perturbations were the following: {−15, 5}, {−9, 10}, and {−5, 15}. The conditional stabilization perturbations were: {15, 5}, {8, 10}, {5, 15}, and {−17, 15}. The termination perturbations were: {−45, 5}, {−35, 10}, and {−65, 2}. The reset perturbations were: {−100, 5} and {−100, 15}. In the DC current simulations (Fig. 8), we stimulated the model with currents ranging between 0 and 0.34 nA and used the SymPy symbolic math module (1.7.1) to compute the Jacobian matrix and to perform a stability analysis of the fixed points. In the cholinergic modulation simulations, we multiplied the Ca_{HVA} maximal conductance with factors ranging from 1 to 1.76 and performed the stability analysis.

Two-compartment model

For the nexus, we used the same system of equations and parameters as in the two-variable reduced model described above (Eqs. 2, 5 in the main text) with $\bar{g}_{Ca_{HVA}} = 4.9$ mS/cm^2 to account for the flow of current to the soma. For the soma, we used the classical Hodgkin–Huxley equations and parameters, taken from the *Mathematical foundations of neuroscience* book (Ermentrout and Terman, 2010). The specific capacitance of the soma was defined as 1 μF/cm^2 and the diameter set to a similar value as the nexus, 18 μm. The axial connection conductance between the two compartments was set to 0.4 mS/cm^2. The example perturbations shown in Figure 9 were introduced 8 ms following the Ca^{2+} spike initiation (excitatory peak current = 1.2 nA and inhibitory peak current = −0.4 nA). In the acetylcholine (ACh) example shown, we used 1.07 multiplier for the Ca_{HVA} maximal conductance.

Results

The Ca^{2+} spike phases

We first set out to characterize how robust and stereotypical the Ca^{2+} spike voltage waveform is. We used a prevalent compartmental model of L5PC (Hay et al., 2011; Shai et al., 2015), initiating Ca^{2+} spikes in its nexus by locally injecting various combinations of step current to the soma and double-exponential current to the nexus, mimicking EPSC. Figure 1*A* shows the morphology of the L5PC model, along with the cellular locations that were stimulated and from which voltage was recorded. An example stimulus with its respective somatic and dendritic voltage traces are shown in Figure 1*B*. An overlay of the generated Ca^{2+} spike voltage waveforms showed that the Ca^{2+} spike could be predominantly divided into three phases: (P1) initiation, (P2)

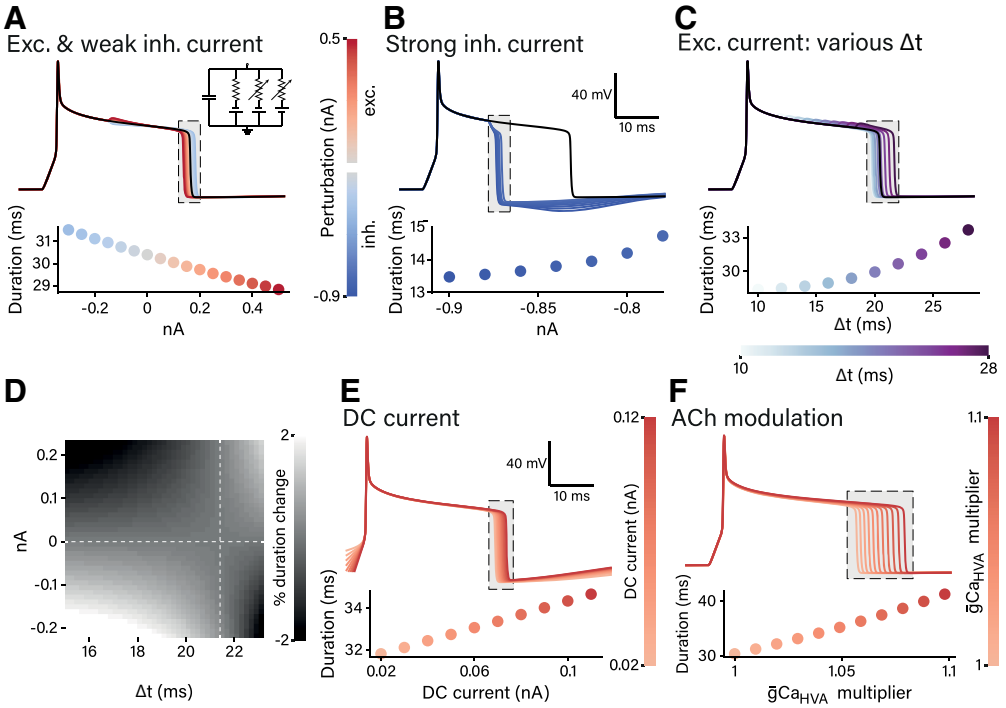

Figure 5. Perturbations and modulations to the Ca^{2+} spike in the two-variable reduced model. ***A***, Changes in Ca^{2+} spike duration following either excitatory or weak inhibitory perturbations 15 ms following the initiation of the spike. Top, Ca^{2+} spike voltage waveforms (black trace: nonperturbation; reds: excitatory perturbations; blues: weak inhibitory perturbations; shaded area: spike termination). Bottom, Spike duration as a function of perturbation amplitude. ***B***, Same as ***A*** with strong inhibitory perturbations. ***C***, Same as ***A*** with excitatory inputs at different perturbation timings. ***D***, Change in Ca^{2+} spike duration (%) across the plane spanned by the perturbation-current peak and the perturbation timing (dashed lines: sign transition in duration). ***E***, Same as ***A*** with constant DC current at various stimulation amplitudes. ***F***, Same as ***A*** with an increase in the Ca_{HVA} conductance.

plateau potential, and (P3) termination (Fig. 1*C*). The initiation phase, in which dendritic depolarized voltage is accumulated, varied in shape according to the stimulation conditions. However, the shape of the large and persistent depolarization, the plateau potential phase that follows the Ca^{2+} spike peak potential, and the shape of the termination phase were robust to different stimulation protocols. We quantified the variability of each phase in response to various input stimulations (Fig. 1*D*). Thus, the typical shape of the plateau and the termination phases of the Ca^{2+} spike across many stimulation protocols suggest that a robust mechanism exists for sustaining the Ca^{2+} spike and the activation of the currents involved.

The effect of external input and cholinergic modulation on L5PC Ca^{2+} spike

We examined how different synaptic perturbations and biophysical conditions shape the typical waveform of the Ca^{2+} spike. First, we perturbed the spike during the plateau potential phase with either an excitatory or inhibitory postsynaptic-like current. First, we noticed that the Ca^{2+} spike is robust to such synaptic perturbations. The perturbations quickly died out and the membrane potential returned to the original trajectory (Fig. 2*A*). Nevertheless, the perturbation did have interesting and counterintuitive effects on the voltage trajectory: at a certain range of perturbation timings, the duration of the Ca^{2+} spike was shortened by an excitatory current during the plateau potential phase, whereas a weak inhibitory current extended it. A strong inhibitory input succeeded in terminating the spike (Fig. 2*B*). When the excitatory current perturbed the Ca^{2+} spike at a later stage of the plateau phase, the perturbation extended the spike duration (Fig. 2*C*). When we plotted the change in Ca^{2+} spike duration as a function of the peak of the double-exponential current and perturbation timing, a saddle-shape effect was revealed (Fig. 2*D*). Note that the effect of the perturbations is independent of the axonal APs (Fig. 2*A*,*B*).

In addition to synaptic perturbations, a tonic depolarization of the membrane potential by a long-step current injection also affected the Ca^{2+} spike (Fig. 2*E*). We injected a DC current step with various intensities to the nexus of a L5PC with axosomatic APs, and recorded the output Ca^{2+} waveform. As the injected current was increased, the Ca^{2+} spike duration increased.

Recently it was experimentally shown that activation of cholinergic axons in the cortex leads to an increased excitability of the nexus (Williams and Fletcher, 2019). This phenomenon is mediated through an increase in the conductance of Ca_{HVA}. To replicate these findings, we increased the conductance of the Ca_{HVA} in the apical dendrites of our model. In accordance with the experimental results, an increase in the Ca_{HVA} conductance extended the duration of the Ca^{2+} spike (Fig. 2*F*). We could also achieve this effect by decreasing the conductance of K^+ channels, a result that was experimentally observed and suggested as a cholinergic mechanism to control dendritic excitability (Friedman et al., 1992; Reuveni et al., 1993; Hoffman et al., 1997; Hoffman and Johnston, 1999; Delmas and Brown, 2005; Buchanan et al., 2010; Giessel and Sabatini, 2010). To conclude, the Ca^{2+} spike, albeit a robust phenomenon, can be modulated by synaptic perturbations, constant current, and changes in dendritic excitability through Ca_{HVA} conductance.

Toward model reduction: the membrane currents involved in the Ca^{2+} spike

The dynamics of the currents involved in the Ca^{2+} spike dictate its response to various perturbations and modulations. Figure 3*A*–*C* shows the Ca^{2+} spike that is generated in the nexus of the

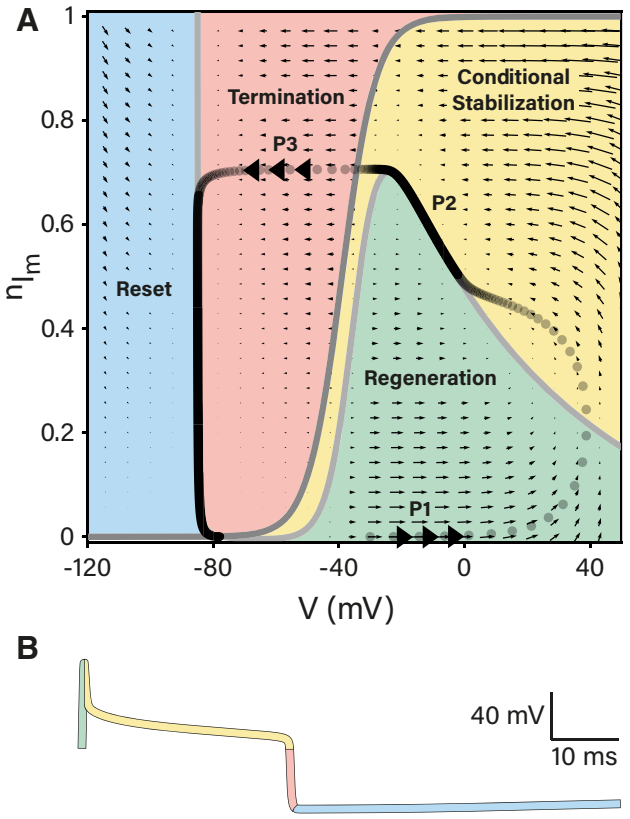

Figure 6. The n_{I_m}-V phase plane of the two-variable reduced nexus model. ***A***, The two-variable dynamical system of n_{I_m} and V, and their nullclines (dark and light gray, respectively). The dynamical regimes are "regeneration" (green), "conditional stabilization" (yellow), "termination" (red), and "reset" (blue). The dynamics flow at each configuration of variables is determined by the size and direction of the derivatives (represented by black arrows). The Ca^{2+} spike trajectory is represented by black semi-transparent circles (a circle every 0.025 ms). The three labeled phases are the initiation (P1), plateau potential (P2), and termination (P3) phases. ***B***, The voltage waveform of the spike is labeled according to the four regimes in ***A***.

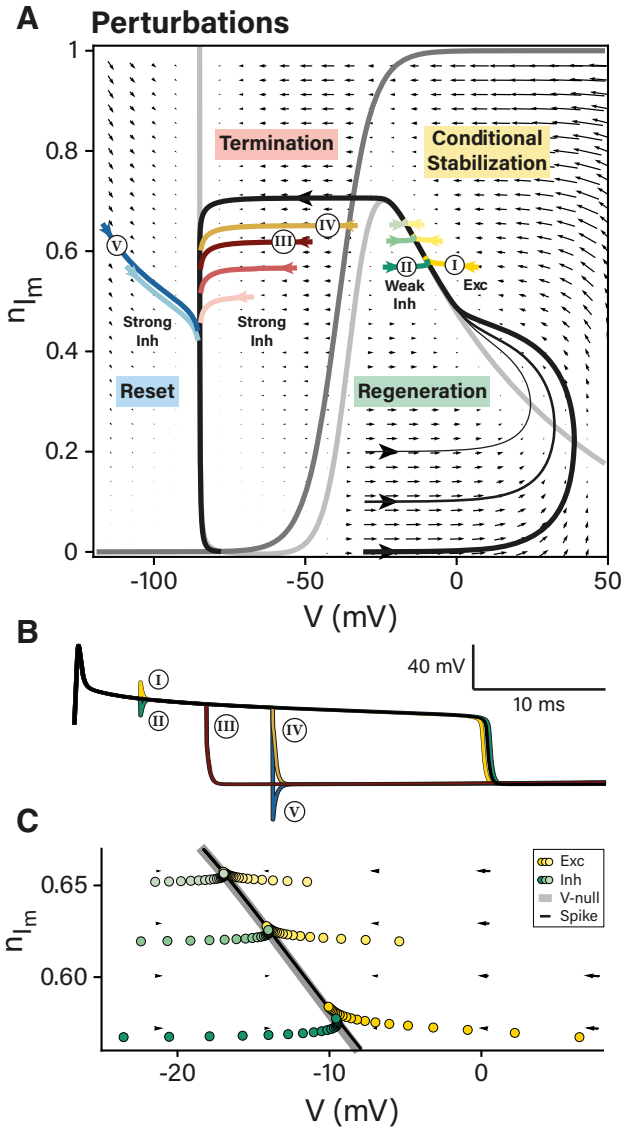

Figure 7. Perturbations of the Ca^{2+} spike in the of n_{I_m}-V phase plane. ***A***, Excitatory and inhibitory perturbations in the n_{I_m}-V phase plane (12 perturbations are shown; for each, the colored trajectory is 1 ms). The perturbations are colored according to the different regimes (greens: "regeneration"; yellows: "conditional stabilization"; reds: "termination"; blues: "reset"). The black lines represent Ca^{2+} spike trajectories that start from three different initial n_{I_m} values. The n_{I_m}-nullcline is in dark gray and the V-nullcline in light gray. The five perturbations that are shown in ***B*** are labeled. ***B***, The Ca^{2+} spike waveforms of the trajectories in ***A*** (black: the bold trajectory; the other five voltage waveforms match the labeled trajectories). ***C***, Zoom-in to the excitatory and weak inhibitory perturbations in ***A***; each perturbation trajectory is 1 ms (a circle every 0.05 ms).

full L5PC compartmental model, and the underlying membrane currents and conductances. The two main currents that are responsible for keeping the plateau potential (P2) and for its subsequent termination (P3) are clearly the Ca_{HVA} current and the slower K^+ current (I_m). The rest of the currents are mainly involved in the initiation of the Ca^{2+} spike (P1). For examining the spike under simpler morphologic conditions, we used a single-compartment iso-potential model that mimics the nexus dynamics (see Materials and Methods). The currents and conductances involved in the Ca^{2+} spike are qualitatively similar both with and without the complete cell morphology (Fig. 3*D*–*F*). Therefore, the morphologically reduced model captures the physiological essence of the Ca^{2+} spike.

A two-variable reduced model

To further understand how various conditions affect the Ca^{2+} spike, we set to reduce the problem not only morphologically, as in Figure 3, but also dynamically. We included in our iso-potential model only the two voltage-dependent currents that are responsible for the plateau and termination phases: the Ca_{HVA} current (consisting of an activation and an inactivation gate) and the I_m (controlled by an activation gate). There are overall four variables for this system of equations: a voltage variable and three gating variables. The dynamic equations of this reduced system are the following (see Materials and Methods for further details):

$$C\frac{dV}{dt} = I_{ext} - \overbrace{g_L(V-E_L)}^{I_{leak}} - \overbrace{\bar{g}_{Ca_{HVA}} m_{Ca_{HVA}}^2 h_{Ca_{HVA}} (V-E_{Ca})}^{I_{Ca_{HVA}}} - \overbrace{\bar{g}_{I_m} n_{I_m} (V-E_K)}^{I_m} \quad (1)$$

$$\frac{dn_{I_m}}{dt} = \alpha_n(V)(1-n_{I_m}) - \beta_n(V) n_{I_m} \quad (2)$$

$$\frac{dm_{Ca_{HVA}}}{dt} = \alpha_m(V)(1-m_{Ca_{HVA}}) - \beta_m(V) m_{Ca_{HVA}} \quad (3)$$

$$\frac{dh_{Ca_{HVA}}}{dt} = \alpha_h(V)(1-h_{Ca_{HVA}}) - \beta_h(V) h_{Ca_{HVA}}. \quad (4)$$

The Ca^{2+} spike generated by this four-variable reduced model as well as the interplay between the gates are both shown

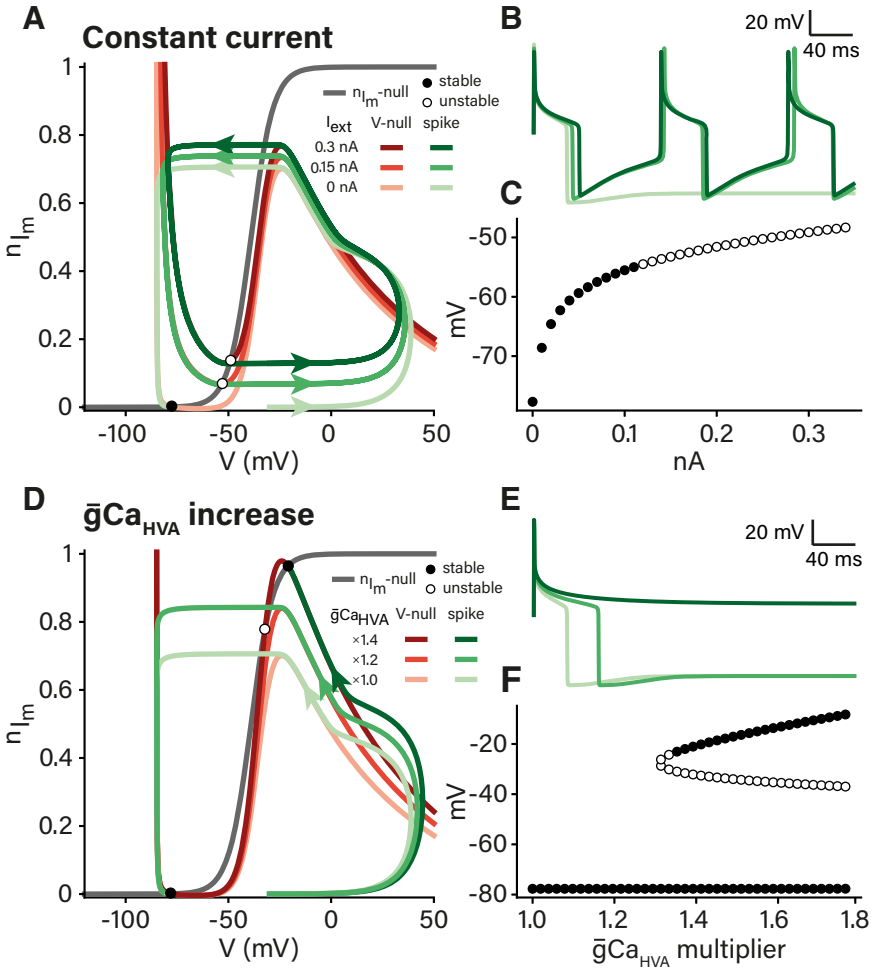

Figure 8. Constant current and Ca_{HVA} conductance affect the n_{I_m}-*V* phase plane. ***A***, The effect of increasing the external constant current on the *V*-nullcline and the Ca^{2+} spike trajectory in the n_{I_m}-*V* phase plane. Darker colors represent higher external tonic currents (reds: *V*-nullcline; greens: Ca^{2+} spike; gray: n_{I_m}-nullcline; black circle: stable fixed points; white circle: unstable fixed points). ***B***, The voltage waveforms of the Ca^{2+} spikes in ***A***. ***C***, The bifurcation diagram of the system; the voltage value of the fixed points as a function of the external constant current (black circle: stable; white circle: unstable). ***D–F*** are the same as ***A–C***, respectively, for increasing the maximum Ca_{HVA} conductance.

in Figure 4. Further reduction of such a system can be obtained using a separation of time scales (Rinzel and Ermentrout, 1989; Izhikevich, 2006). Figure 4*A*,*B* focus on the time constants and the activation curves of the gating variables in this system (see Materials and Methods). The time constant of the inactivation gate of the Ca^{2+} conductance $h_{Ca_{HVA}}$ is too slow to take part in the Ca^{2+} spike process and can, therefore, be considered as constant. Thus, the only gates that control the spike's dynamics are the activation of the Ca^{2+} conductance $m_{Ca_{HVA}}$ and the activation of the K^+ conductance n_{I_m}. The time constant of the Ca^{2+} activation variable $m_{Ca_{HVA}}$ is an order of magnitude faster than the one of n_{I_m}. The maximum value of the $m_{Ca_{HVA}}$ time constant is around 7 ms, whereas at a similar voltage, the maximum value of the n_{I_m} time constant is around 50 ms. The Ca^{2+} spike generated by the four-variable reduced model and the interplay between the gates are shown in Figure 4*C*,*D*. This reduced model gives insights to the slow dynamics of the plateau potential phase of the spike. When the spike is initiated, the $m_{Ca_{HVA}}$ gate opens immediately. However, because of the time constant of the n_{I_m} gate, it opens slowly (without reaching a fully open state). In this process, the outward current (I_m + I_{leak}) slightly overcomes the inward Ca_{HVA} current through the whole plateau-potential dynamics. Thus, the voltage decreases and the $m_{Ca_{HVA}}$ gate gradually closes, as dictated by its activation curve. An active termination occurs when the voltage membrane potential reaches the point at which the activation curve of the $m_{Ca_{HVA}}$ gate steeply decreases. The n_{I_m} gate reacts to this drop in voltage with a delay (but faster than the opening) until the resting membrane potential is reached. The dynamics of the Ca^{2+} spike imply that we can approximate it by an instantaneous activation for the $m_{Ca_{HVA}}$ gate ($m_{Ca_{HVA}}(V,t) \rightarrow m_{Ca_{HVA}\infty}(V)$). Taking this together with the assumption of a constant inactivation of the $h_{Ca_{HVA}}$ gate ($h_{Ca_{HVA}}(V,t) \rightarrow h_{Ca_{HVA}\infty}(V_0)$), we reach a reduced model with only two dynamical variables. This minimal model can be expressed by the membrane voltage and the n_{I_m} activation gate (Fig. 4*E*,*F*):

$$C\frac{dV}{dt} = I_{ext} - g_L(V - E_L) - \bar{g}_{Ca_{HVA}} m_{Ca_{HVA}\infty}(V) h_{Ca_{HVA}\infty}(V_0)(V - E_{Ca}) - \bar{g}_{I_m} n_{I_m}(V - E_K) \quad (5)$$

$$\frac{dn_{I_m}}{dt} = \alpha_n(V)(1 - n_{I_m}) - \beta_n(V) n_{I_m}.$$

This simplified model has only two biologically meaningful dynamical variables but is sufficient for replicating the Ca^{2+}

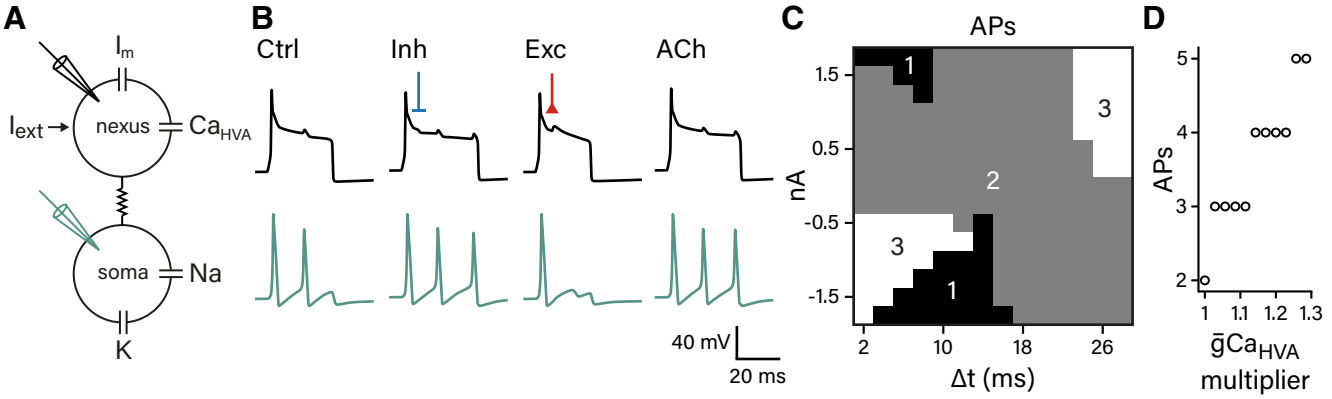

Figure 9. Effect of Ca^{2+} spike perturbations on somatic APs. ***A***, A two-compartment model composed of the reduced nexus attached to a soma with Hodgkin–Huxley channels. ***B***, Voltage traces from the nexus (black) and the soma (teal) in control condition, weak inhibition ($\Delta t = 8$ ms; perturbation peak = −0.4 nA), excitation ($\Delta t = 8$ ms; perturbation peak = 1.2 nA), and ACh condition ($\bar{g}_{Ca_{HVA}}$ multiplier = 1.07). ***C***, Summary of the number of APs as function of the peak perturbation current and timing (black = 1 APs; gray = 2 APs; white = 3 APs). ***D***, Summary of the number of APs as the conductance of the Ca_{HVA} channel is increased.

spike dynamics and its responses to external interventions (as described below).

Perturbations and modulations to the two-variable model

Our reduced model, consisting of two biologically meaningful dynamic variables, qualitatively replicates the reaction of the L5PC Ca^{2+} spike to the various perturbations and modulations. Figure 5*A* shows the effect of excitatory and weak inhibitory current perturbations 15 ms postinitiation of the Ca^{2+} spike, during the plateau potential phase. As in the L5PC (Fig. 2*A*), the spike is robust to such perturbations, while the excitatory input shortened it and the inhibitory input extended it. However, as can be seen in Figure 5*B*, strong inhibition terminated the spike. Note that in this figure, as opposed to Figure 2*B*, the termination dynamics is more abrupt. This is because of both channel dynamics and dendritic morphology. In Figure 5*B*, not only that the model consists of only two currents (I_m and Ca_{HVA}), the $m_{Ca_{HVA}}$ is instantaneous which dramatically restricts the termination dynamics of the spike. Moreover, cell morphology also plays a role in this. During the Ca^{2+} spike, the capacitance of the dendrites is charged. When specific neighboring dendrites are being inhibited, the noninhibited sections are now discharged such that they become a current source for the inhibited dendrites. Thus, axial currents can rapidly flow into the stimulated dendrites. This process slows down the hyperpolarization and elongates the termination phase. This cannot occur in the reduced model, where no dendritic tree exists. When the excitatory perturbation arrived toward the end of the spike, it extended it rather than shortening it (Fig. 5*C*,*D*). Additionally, different levels of tonic current injection levels evoked Ca^{2+} spikes of different durations. As the current level increased, the spike duration was longer (Fig. 5*E*). Finally, higher levels of $\bar{g}_{Ca_{HVA}}$ increased the Ca^{2+} spike duration in a similar way to the effect in our L5PC model (and similarly, we could also extend the spike duration with lower levels of $\bar{g}_{I_m}$ in the two-variable model). To conclude, the perturbations and modulations to the Ca^{2+} spike in the two-variable reduced model showed similar effects as in the L5PC. Further analysis of the spike in this system can help us achieve a better understanding of spike responses and their robust nature.

Dynamical system underlying the Ca^{2+} spike

We can now examine the effect of synaptic perturbations and modulations on the Ca^{2+} spike in a 2D dynamical system that includes the two biologically meaningful variables as discussed above. Previous studies have used different aspects of dynamical systems to examine plateau potentials in cells (FitzHugh, 1960; Noble and Tsien, 1969; Morris and Lecar, 1981; Rinzel and Ermentrout, 1989; Reuveni et al., 1993; Pinsky and Rinzel, 1994; Izhikevich, 2006; Yi et al., 2017). However, a rigorous and specific examination of the Ca^{2+} spike mechanism along with the effect of perturbations and modulations to it, have not been addressed. Figure 6*A* depicts the phase plane of the system which consists of the V and n_{I_m} nullclines (where their derivatives with respect to time equal 0), the dynamical regimes constructed by the nullclines (defined by the direction of the variable derivatives), and the Ca^{2+} spike trajectory. The intersection of the nullclines is the fixed point of the system (the resting membrane potential). The phase plane is divided by the nullclines into four regimes that control the spike trajectory: (1) regeneration, (2) conditional stabilization, (3) termination, and (4) reset. The first regime is the "regeneration" regime, in which the value combination of V and n_{I_m} generates a spike or revives it in the case of a perturbation. Once the spike is generated, it passes quickly through this regime until reaching maximum voltage while opening the n_{I_m} gate. The second regime, the "conditional stabilization" regime, is the basis for the spike robustness and is greatly dependent on the value of n_{I_m} gating variable. In this regime, the plateau potential occurs because of the dynamics of the model variables: The Ca^{2+} spike is quickly "pushed" (horizontally) toward the V-nullcline ($dV/dt > dn_{I_m}/dt$), and the spike slowly crawls along the nullcline because of the small positive value of dn_{I_m}/dt. This stabilization phenomenon occurs only if the n_{I_m} dynamical variable is in relatively low values (low enough so that the trajectory is pushed back toward the V-nullcline). Once the n_{I_m} is higher than its value at the peak of the inverted U-shape ("the hill") of the V-nullcline, which happens around −20 mV, the spike can no longer be stabilized and is closed. The third regime is the "termination" regime, in which all combination pairs close the spike. Finally, the "reset" regime is responsible for setting the n_{I_m} gate back to 0, and V back to the resting potential, i.e., the stable fixed-point of the system under these conditions. The steep slope of the leftmost part of the V-nullcline is the reason that almost no afterhyperpolarization exists. Using a dynamical system for dissecting the Ca^{2+} spike trajectory is not only beneficial for understanding the mechanism of the spike, but it will also enable us to predict its response to various perturbations and modulations.

Perturbations and modulations to the Ca^{2+} spike are explained by the dynamical system

Given the n_{I_m}-V phase-plane representation of the dynamics of the Ca^{2+} spike, we examined the behavior of the perturbations and modulations from Figures 2, 5 in it. First, we considered the effects of various instantaneous excitatory and inhibitory perturbations (Fig. 7*A*; some of the trajectories are fully shown in Fig. 7*B*). We introduce the perturbations in the plateau potential phase (shortly after the spike initiation). An excitatory perturbation increases the membrane voltage and "pulls" the trajectory away from the V-nullcline into the "conditional stabilization" regime. This takes the system to an area with larger time derivatives that "push" the system back toward the nullcline, but faster. Consequently, the Ca^{2+} spike returns to its original trajectory, and the overall spike duration becomes shorter (Fig. 7*C*). Thus, despite a "longer path" introduced by the perturbation, the larger derivatives mean a "faster velocity" and the overall duration for traveling this path becomes shorter. With a weak inhibitory perturbation, the opposite effect occurs: the duration is extended because of the perturbation path and the smaller derivatives along it. However, with strong enough inhibitory perturbation, the Ca^{2+} spike trajectory crosses the hill of the V-nullcline, enters the termination regime, and the spike is terminated. This observation explains the sharp boundary between inhibitory inputs that will be recovered and will not affect the spike much, and those that will terminate it (for comparison, see Doron et al., 2017).

The introduction of a constant tonic DC current changes the shape of the V-nullcline (Fig. 8*A*). The nullcline is shifted up vertically and becomes more curved near the fixed point. The matching voltage traces are shown in Figure 8*B*. Strong enough current changes the stability of the fixed point from a stable to an unstable fixed point (Fig. 8*C*), and introduces a limit-cycle state. In this state, we obtain the experimentally observed regular train of Ca^{2+} spikes (Amitai et al., 1993). Note that in Figure 5*A–D*, when we introduced the double-exponent current, we, in fact, changed the V-nullcline instantaneously. In this way, the voltage trajectory followed the instantaneous nullcline and we could elongate the spike when the perturbation was introduced at a late stage of the plateau. Increasing the Ca_{HVA} conductance, imitating the effect of ACh, results in an upwards elongation of the V-nullcline "hill" (Fig. 8*D*). Interestingly, the nullclines of n_{I_m} and V are nearly parallel along a significant portion of the phase plane. As a result, increasing the Ca_{HVA} conductance stretches the V-nullcline along this parallel region. This effectively increases the duration of the plateau potential phase (Fig. 8*E*). The parallel nature of the two nullclines allows for a wide dynamic range of ACh modulation without qualitatively affecting the dynamics of the system. A strong enough increase in the Ca_{HVA} conductance, however, introduces two new fixed points (Fig. 8*F*). As $\bar{g}_{Ca_{HVA}}$ is increased, the middle range of the V-nullcline (between −40 and −20 mV) becomes steeper, and therefore for small range of conductance values ($\bar{g}_{Ca_{HVA}}$ multiplier: 1.31–1.33) both fixed points are unstable, and above this range one is unstable and the other is stable. Thus, the spike in the model, which lacks an inactivation gate, stays stuck at high voltage. These new fixed points could be the basis for plateau potentials with much longer dynamics than the regular Ca^{2+} spike that were reported in the literature (Larkum et al., 2001; Gambino et al., 2014; Stuart and Spruston, 2015).

To observe the effects that the current perturbation and cholinergic modulation have on the output of the cell, we constructed a two-compartment model with a nexus attached to a soma (Fig. 9*A*). The model consisted of our reduced nexus with Ca_{HVA} and I_m channels and a soma with voltage-dependent Na^+ and K^+ currents of the Hodgkin–Huxley model (Hodgkin and Huxley, 1952). Figure 9*B* shows example traces of the dendritic-compartment Ca^{2+} spikes and the Na^+-based APs generated at the soma. In the control condition, in the absence of external perturbation, the Ca^{2+} spike caused a burst of two somatic APs. Weak inhibition 8 ms following the initiation of the Ca^{2+} spike slightly extended the duration of the nexus Ca^{2+} spike, which subsequently added another somatic AP; however, strong enough and timed excitatory input was able to eliminate one somatic AP. Cholinergic modulation (modeled by an increase of the nexus $\bar{g}_{Ca_{HVA}}$) caused the number of somatic APs to increase. A summary of the number of generated APs as a function of the perturbation-current peak and the perturbation timing is shown in Figure 9*C*. The results are in line with the effects on the Ca^{2+} spike observed in Figure 5. Overall, early weak inhibition as well as late excitation resulted with more APs; however, strong inhibition as well as early excitation resulted with less APs. Figure 9*D* shows the increase in the number of somatic APs as the level of ACh is increased. To conclude, we saw that the observed effect on the Ca^{2+} spike duration could have significant implications on the number of somatic APs. Thus, interventions in the Ca^{2+} spike can directly affect the output signal of the neuron.

Discussion

The dendritic Ca^{2+} spike is a well-explored phenomenon of pyramidal cells in the cortex and hippocampus as well as in Purkinje cells in the cerebellum. However, the underlying mechanism that controls the spike, as well as the way various factors affect it, are not fully understood. Here, we identified the two main currents (Ca_{HVA} and I_m) that control the plateau potential phase of the spike and obtained a morphologically and physiologically reduced model that replicated it. This model includes two interpretable and biological dynamic variables (V and n_{I_m}), which allowed us to closely examine the spike responses to various perturbations and modulations and the interactions between the variables. The trajectory of the Ca^{2+} spike in a 2D phase plane provides us with insights into ways to regulate and modulate the dendritic spike, and by that to directly change the cell's output.

Robustness of the Ca^{2+} spike

We identified four regions in the n_{I_m}-V phase plane: "regeneration," "conditional stabilization," "termination," and "reset." In the "conditional stabilization" regime, the strong voltage derivatives, relative to the n_{I_m} ones, "push" the spike toward the V-nullcline, where the derivatives are small. This generates the crawling dynamics along the V-nullcline and the slow plateau potential phase. This is the source of the apparent stability of the plateau potential. At this stage, many types of perturbations may affect the spike, but its general trajectory is preserved, even in response to relatively large perturbations. Weak inhibitory instantaneous perturbations move the spike to the "regeneration" region and the spike returns to its trajectory. Excitatory instantaneous perturbations bring the spike to the "conditional stabilization" region, from which the spike also quickly returns to its trajectory. It is important to realize that in a cell with a realistic morphology, the effect of perturbations is more complex. With a realistic morphology the spatial and temporal specificity of the perturbation

plays a crucial role. Unlike NMDA spikes, which locally occur in a specific dendritic branch and are easier to regulate (Larkum et al., 2009; Doron et al., 2017), Ca^{2+} spikes are a spatially broader phenomenon and therefore terminating it requires a strong temporally coherent inhibitory synaptic input. An acute focal space-limited inhibition will have a more minor effect on the Ca^{2+} spike, as other dendrites can serve as a current source to the inhibited cell section to compensate for the perturbation. Note that inhibitory synaptic inputs may have a much stronger effect during the initiation phase of the Ca^{2+} spike (Larkum et al., 1999; Palmer et al., 2012), an effect that was not studied here.

In addition to this robustness to perturbation, the shape of the Ca^{2+} spike is also robust to changes in Ca_{HVA} conductance. This interesting phenomenon stems from the nearly parallel lines in the middle range of the V-nullcline and the n_{I_m}-nullcline (between −40 and −20 mV). As observed in Figure 8*D*, an increase in Ca_{HVA} conductance elongates the duration of the plateau phase of the Ca^{2+} spike by an increase in the V-nullcline hill. If the angle between the lines was smaller, there would be a narrower dynamic range for changes in conductance before another stable fixed point would be created by the intersection of the nullclines. Therefore, ACh, which modulates Ca_{HVA} conductance in the apical dendrites (Williams and Fletcher, 2019), can control the Ca^{2+} spike waveform in a precise manner. It may be tempting to think about this new stable fixed point as a spurious fixed point, as the membrane potential cannot get stuck in high membrane potential values. However, this fixed point may explain the long tonic potentials observed in several studies (Larkum and Zhu, 2002; Lee et al., 2012; Bittner et al., 2017), and since the channels do inactivate (albeit slowly), the inactivation will eventually force the termination of these long potentials.

Although the initiation of a Ca^{2+} spike involves many currents, our analysis explicitly indicates the effect of channel recovery on the generation of a subsequent spike. The duration, as well as the initiation threshold, are closely dependent on the time from the previous Ca^{2+} spike. As can be seen in Figure 6, because of the V-nullcline shape, a subsequent spike is predicted to be shorter and should require more current for initiation. The influence of the previous Ca^{2+} spike becomes weaker as the spike progresses toward to the resting membrane potential and the channels are in the process of recovery. In this way, variability in the duration of the Ca^{2+} spike can be introduced.

Model assumptions and limitations

Our analysis of the main currents involved in the Ca^{2+} spike pointed out the I_m and Ca_{HVA} currents. This conclusion is dependent on the voltage-dependent conductances used during the optimization process of the L5PC model by Hay et al. (2011). It should be noted that the role I_m has in our analysis can be replaced with any voltage-dependent or Ca^{2+}-dependent K^+ channel that has an order of magnitude longer time constant than that of the Ca_{HVA} channel in the apical dendritic tree of a pyramidal cell. For example, BK-type Ca^{2+}-dependent K^+-channel (Golding et al., 1999; Bock and Stuart, 2016), which opens because of the Ca^{2+} influx during the spike, could take the role of I_m in our model. However, such Ca^{2+}-dependent K^+ would likely preclude the 2D phase-plane analysis as the relation between K^+ current and voltage would be more complex.

In this work, we examined analytically the effect of perturbations and modulations on the Ca^{2+} spike. Static variables, such as the structure of the cell, its dendritic load, and the level of soma-nexus coupling, also have a significant influence on the spike (Larkum et al., 1999; Vetter et al., 2001; Schaefer et al., 2003; Galloni et al., 2020); however, the inclusion of geometrical aspects of the cell requires a high dimensional system, which is not amenable for phase-plane analysis. In addition, in this study, we focused on the plateau potential and termination phases of the spike. The initiation phase, which is highly stimulus-specific and involves more ion-channels, is beyond the scope of this work and should be further examined. We saw that an increase in Ca_{HVA} conductance increases the duration of the spike. However, different phases can be a target to other modulatory interferences. For example, it is expected that the initiation phase will involve I_h (Harnett et al., 2015; Labarrera et al., 2018), and therefore, norepinephrine may serve as the initiation probability "knob," whereas ACh is the duration "knob" that comes into play once the spike was generated. The difference in cholinergic control on the soma and the apical dendrites (Williams and Fletcher, 2019) suggests that local cholinergic control may participate in such mechanisms. An example for a potential source are local cortical $VIP^+/ChAT^+$ interneurons that project to layer 1 of the cortex (Obermayer et al., 2019; Dudai et al., 2020, 2021; Granger et al., 2020). Future work should closely examine the relationship between the spike properties and the ionic currents flowing in and out of the cell, and specifically Ca^{2+} currents.

Any perturbation or modulation of the Ca^{2+} spike affects the amount of Ca^{2+} that enters the cell, and therefore is likely to directly affect synaptic plasticity (Golding et al., 2002; Kampa et al., 2006; Bar Ilan et al., 2011; Bittner et al., 2017). For example, our results indicate that the specific timing of synaptic input relative to the Ca^{2+} spike initiation may change its duration, suggesting a new type of spike-timing-dependent plasticity mechanism for distal synapses, which could lead to an enhancement or reduction of synapses. This capacity to regulate the spike duration may introduce a fine-tuning mechanism for learning rules in cortical networks and increase subtleties that are not addressed by Hebbian plasticity rules (Froemke et al., 2005; Sjöström and Häusser, 2006; Magee and Grienberger, 2020; Bicknell and Häusser, 2021). Additionally, this variability in duration may also have significant functional implications on animal perception. Longer spike durations mean longer amplification of distal synapses, supporting the association between top-down and sensory information (Larkum, 2013; Suzuki and Larkum, 2020). Dendritic Ca^{2+} events in L5PCs directly affect perceptual detection tasks in mice, promoting communication with sub-cortical areas (Takahashi et al., 2016, 2020), and regulating this mechanism will be beneficial for precise sensory interactions of the animal with its environment.

The Ca^{2+} spike is a prominent event in the activity of the pyramidal neuron, which has a significantly longer timescale than the millisecond axonal APs. In this work, we explain the mechanism for the robustness of the Ca^{2+} spike and suggest ways to control its final waveform. These natural perturbations have clear effect on the output of the neuron as demonstrated in Figure 9.

References

Adams PR, Brown DA, Constanti A (1982) M-currents and other potassium currents in bullfrog sympathetic neurones. J Physiol 330:537–572.

Amitai Y, Friedman A, Connors BW, Gutnick MJ (1993) Regenerative activity in apical dendrites of pyramidal cells in neocortex. Cereb Cortex 3:26–38.

Bar Ilan L, Gidon A, Segev I (2011) Interregional synaptic competition in neurons with multiple STDP-inducing signals. J Neurophysiol 105:989–998.

Bicknell BA, Häusser M (2021) A synaptic learning rule for exploiting nonlinear dendritic computation. Neuron 109:1–17.

Bittner KC, Milstein AD, Grienberger C, Romani S, Magee JC (2017) Behavioral time scale synaptic plasticity underlies CA1 place fields. Science 357:1033–1036.

Bock T, Stuart GJ (2016) The impact of BK channels on cellular excitability depends on their subcellular location. Front Cell Neurosci 10:206.

Buchanan KA, Petrovic MM, Chamberlain SEL, Marrion NV, Mellor JR (2010) Facilitation of long-term potentiation by muscarinic M(1) receptors is mediated by inhibition of SK channels. Neuron 68:948–963.

Carnevale TN, Hines ML (2006) The NEURON book. Cambridge: Cambridge University Press.

Delmas P, Brown DA (2005) Pathways modulating neural KCNQ/M (Kv7) potassium channels. Nat Rev Neurosci 6:850–862.

Doron M, Chindemi G, Muller E, Markram H, Segev I (2017) Timed synaptic inhibition shapes NMDA spikes, influencing local dendritic processing and global I/O properties of cortical neurons. Cell Rep 21:1550–1561.

Dudai A, Yayon N, Lerner V, Tasaka G, Deitcher Y, Gorfine K, Niederhoffer N, Mizrahi A, Soreq H, London M (2020) Barrel cortex VIP/ChAT interneurons suppress sensory responses in vivo. PLoS Biol 18:e3000613.

Dudai A, Yayon N, Soreq H, London M (2021) Cortical VIP^{+}/$ChAT^{+}$ interneurons: from genetics to function. J Neurochem 158:1320–1333.

Ermentrout GB, Terman DH (2010) Mathematical foundations of neuroscience, interdisciplinary applied mathematics. New York: Springer.

FitzHugh R (1960) Thresholds and plateaus in the Hodgkin-Huxley nerve equations. J Gen Physiol 43:867–896.

Fletcher LN, Williams SR (2019) Neocortical topology governs the dendritic integrative capacity of layer 5 pyramidal neurons. Neuron 101:76–90.e4.

Friedman A, Arens J, Heinemann U, Gutnick MJ (1992) Slow depolarizing afterpotentials in neocortical neurons are sodium and calcium dependent. Neurosci Lett 135:13–17.

Froemke RC, Poo MM, Dan Y (2005) Spike-timing-dependent synaptic plasticity depends on dendritic location. Nature 434:221–225.

Galloni AR, Laffere A, Rancz E (2020) Apical length governs computational diversity of layer 5 pyramidal neurons. Elife 9:e55761.

Gambino F, Pagès S, Kehayas V, Baptista D, Tatti R, Carleton A, Holtmaat A (2014) Sensory-evoked LTP driven by dendritic plateau potentials in vivo. Nature 515:116–119.

Gidon A, Segev I (2012) Principles governing the operation of synaptic inhibition in dendrites. Neuron 75:330–341.

Giessel AJ, Sabatini BL (2010) M1 muscarinic receptors boost synaptic potentials and calcium influx in dendritic spines by inhibiting postsynaptic SK channels. Neuron 68:936–947.

Golding NL, Jung HY, Mickus T, Spruston N (1999) Dendritic calcium spike initiation and repolarization are controlled by distinct potassium channel subtypes in CA1 pyramidal neurons. J Neurosci 19:8789–8798.

Golding NL, Staff NP, Spruston N (2002) Dendritic spikes as a mechanism for cooperative long-term potentiation. Nature 418:326–331.

Granger AJ, Wang W, Robertson K, El-Rifai M, Zanello AF, Bistrong K, Saunders A, Chow BW, Nuñez V, García MT, Harwell CC, Gu C, Sabatini BL (2020) Cortical ChAT+ neurons co-transmit acetylcholine and GABA in a target- and brain-region-specific manner. Elife 9:e57749.

Harnett MT, Xu NL, Magee JC, Williams SR (2013) Potassium channels control the interaction between active dendritic integration compartments in layer 5 cortical pyramidal neurons. Neuron 79:516–529.

Harnett MT, Magee JC, Williams SR (2015) Distribution and function of HCN channels in the apical dendritic tuft of neocortical pyramidal neurons. J Neurosci 35:1024–1037.

Hay E, Hill S, Schürmann F, Markram H, Segev I (2011) Models of neocortical layer 5b pyramidal cells capturing a wide range of dendritic and perisomatic active properties. PLoS Comput Biol 7:e1002107.

Hodgkin AL, Huxley AF (1952) A quantitative description of membrane current and its application to conduction and excitation in nerve. J Physiol 117:500–544.

Hoffman DA, Johnston D (1999) Neuromodulation of dendritic action potentials. J Neurophysiol 81:408–411.

Hoffman DA, Magee JC, Colbert CM, Johnston D (1997) K+ channel regulation of signal propagation in dendrites of hippocampal pyramidal neurons. Nature 387:869–875.

Izhikevich EM (2006) Dynamical systems in neuroscience: the geometry of excitability and bursting. Cambridge: The MIT Press.

Kampa BM, Letzkus JJ, Stuart GJ (2006) Requirement of dendritic calcium spikes for induction of spike-timing-dependent synaptic plasticity. J Physiol 574:283–290.

Labarrera C, Deitcher Y, Dudai A, Weiner B, Kaduri Amichai A, Zylbermann N, London M (2018) Adrenergic modulation regulates the dendritic excitability of layer 5 pyramidal neurons in vivo. Cell Rep 23:1034–1044.

Larkum M (2013) A cellular mechanism for cortical associations: an organizing principle for the cerebral cortex. Trends Neurosci 36:141–151.

Larkum ME, Zhu JJ (2002) Signaling of layer 1 and whisker-evoked Ca2+ and Na+ action potentials in distal and terminal dendrites of rat neocortical pyramidal neurons in vitro and in vivo. J Neurosci 22:6991–7005.

Larkum ME, Zhu JJ, Sakmann B (1999) A new cellular mechanism for coupling inputs arriving at different cortical layers. Nature 398:338–341.

Larkum ME, Zhu JJ, Sakmann B (2001) Dendritic mechanisms underlying the coupling of the dendritic with the axonal action potential initiation zone of adult rat layer 5 pyramidal neurons. J Physiol 533:447–466.

Larkum ME, Nevian T, Sandler M, Polsky A, Schiller J (2009) Synaptic integration in tuft dendrites of layer 5 pyramidal neurons: a new unifying principle. Science 325:756–760.

Lee D, Lin BJ, Lee AK (2012) Hippocampal place fields emerge upon single-cell manipulation of excitability during behavior. Science 337:849–853.

Leleo EG, Segev I (2021) Burst control: synaptic conditions for burst generation in cortical layer 5 pyramidal neurons. PLoS Comput Biol 17: e1009558.

Magee JC, Grienberger C (2020) Synaptic plasticity forms and functions. Annu Rev Neurosci 43:95–117.

Major G, Larkum ME, Schiller J (2013) Active properties of neocortical pyramidal neuron dendrites. Annu Rev Neurosci 36:1–24.

Morris C, Lecar H (1981) Voltage oscillations in the barnacle giant muscle fiber. Biophys J 35:193–213.

Noble D, Tsien RW (1969) Reconstruction of the repolarization process in cardiac Purkinje fibres based on voltage clamp measurements of membrane current. J Physiol 200:233–254.

Obermayer J, Luchicchi A, Heistek TS, de Kloet SF, Terra H, Bruinsma B, Mnie-Filali O, Kortleven C, Galakhova AA, Khalil AJ, Kroon T, Jonker AJ, de Haan R, van de Berg WDJ, Goriounova NA, de Kock CPJ, Pattij T, Mansvelder HD (2019) Prefrontal cortical ChAT-VIP interneurons provide local excitation by cholinergic synaptic transmission and control attention. Nat Commun 10:5280.

Palmer LM, Schulz JM, Murphy SC, Ledergerber D, Murayama M, Larkum ME (2012) The cellular basis of GABA(B)-mediated interhemispheric inhibition. Science 335:989–993.

Pérez-Garci E, Larkum ME, Nevian T (2013) Inhibition of dendritic Ca2+ spikes by GABAB receptors in cortical pyramidal neurons is mediated by a direct Gi/o-β-subunit interaction with Cav1 channels. J Physiol 591:1599–1612.

Pinsky PF, Rinzel J (1994) Intrinsic and network rhythmogenesis in a reduced traub model for CA3 neurons. J Comput Neurosci 1:39–60.

Poleg-Polsky A (2019) Dendritic spikes expand the range of well tolerated population noise structures. J Neurosci 39:9173–9184.

Reuveni I, Friedman A, Amitai Y, Gutnick MJ (1993) Stepwise repolarization from Ca2+ plateaus in neocortical pyramidal cells: evidence for nonhomogeneous distribution of HVA Ca2+ channels in dendrites. J Neurosci 13:4609–4621.

Rinzel J, Ermentrout GB (1989) Analysis of neural excitability and oscillations. In: Methods in neuronal modeling (Koch C, Segev I, eds). Cambridge: The MIT Press.

Schaefer AT, Larkum ME, Sakmann B, Roth A (2003) Coincidence detection in pyramidal neurons is tuned by their dendritic branching pattern. J Neurophysiol 89:3143–3154.

Schiller J, Schiller Y, Stuart G, Sakmann B (1997) Calcium action potentials restricted to distal apical dendrites of rat neocortical pyramidal neurons. J Physiol 505:605–616.

Shai AS, Anastassiou CA, Larkum ME, Koch C (2015) Physiology of layer 5 pyramidal neurons in mouse primary visual cortex: coincidence detection through bursting. PLoS Comput Biol 11:e1004090.

Sjöström PJ, Häusser M (2006) A cooperative switch determines the sign of synaptic plasticity in distal dendrites of neocortical pyramidal neurons. Neuron 51:227–238.

Spruston N (2008) Pyramidal neurons: dendritic structure and synaptic integration. Nat Rev Neurosci 9:206–221.
Stuart GJ, Häusser M (2001) Dendritic coincidence detection of EPSPs and action potentials. Nat Neurosci 4:63–71.
Stuart GJ, Sakmann B (1994) Active propagation of somatic action potentials into neocortical pyramidal cell dendrites. Nature 367:69–72.
Stuart GJ, Spruston N (2015) Dendritic integration: 60 years of progress. Nat Neurosci 18:1713–1721.
Suzuki M, Larkum ME (2020) General anesthesia decouples cortical pyramidal neurons. Cell 180:666–676.e13.
Takahashi N, Oertner TG, Hegemann P, Larkum ME (2016) Active cortical dendrites modulate perception. Science 354:1587–1590.
Takahashi N, Ebner C, Sigl-Glöckner J, Moberg S, Nierwetberg S, Larkum ME (2020) Active dendritic currents gate descending cortical outputs in perception. Nat Neurosci 23:1277–1285.
Vetter P, Roth A, Häusser M (2001) Propagation of action potentials in dendrites depends on dendritic morphology. J Neurophysiol 85:926–937.
Williams SR, Fletcher LN (2019) A dendritic substrate for the cholinergic control of neocortical output neurons. Neuron 101:486–499.e4.
Yi G, Wang J, Wei X, Deng B (2017) Action potential initiation in a two-compartment model of pyramidal neuron mediated by dendritic Ca2+ spike. Sci Rep 7:45684.